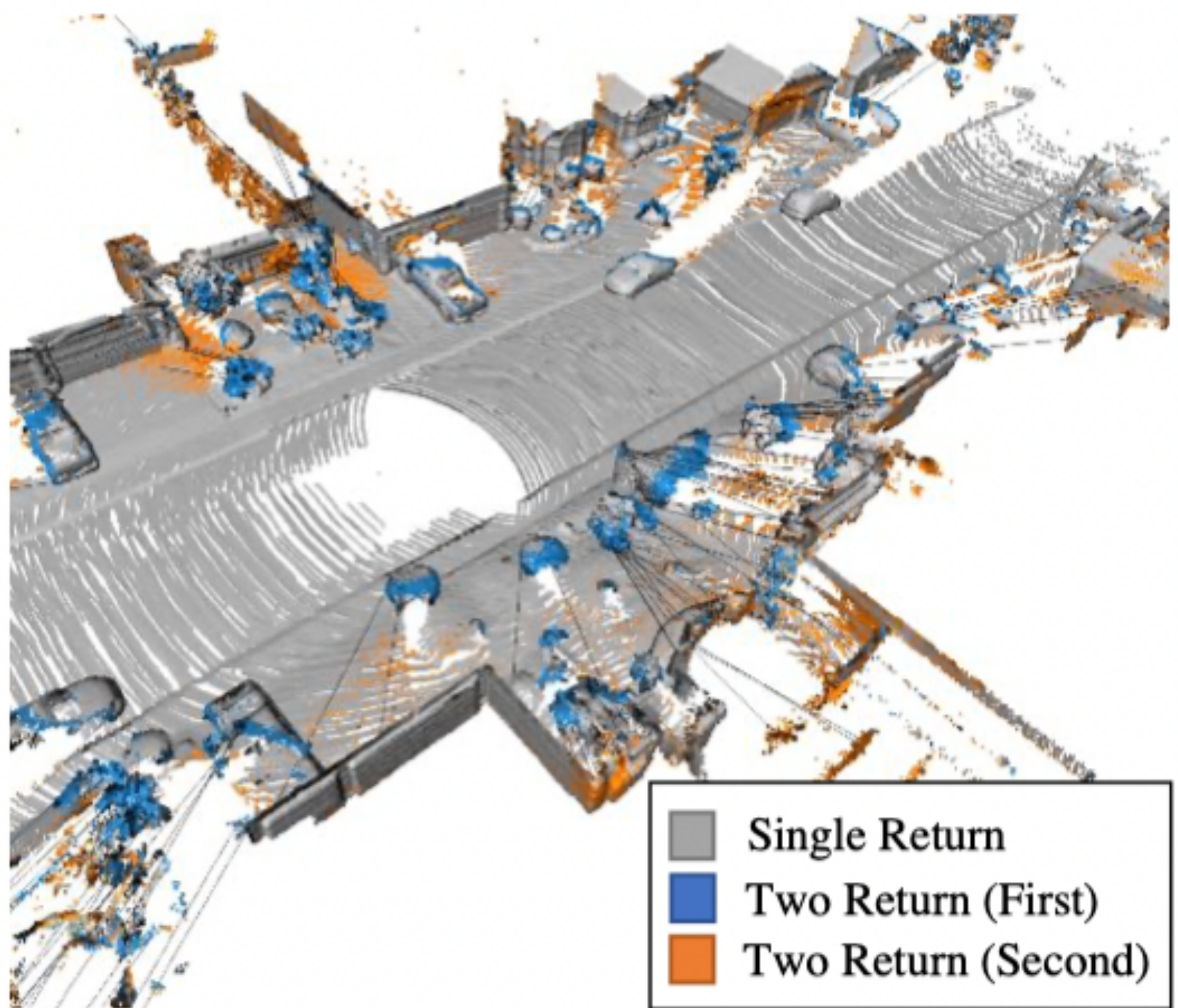


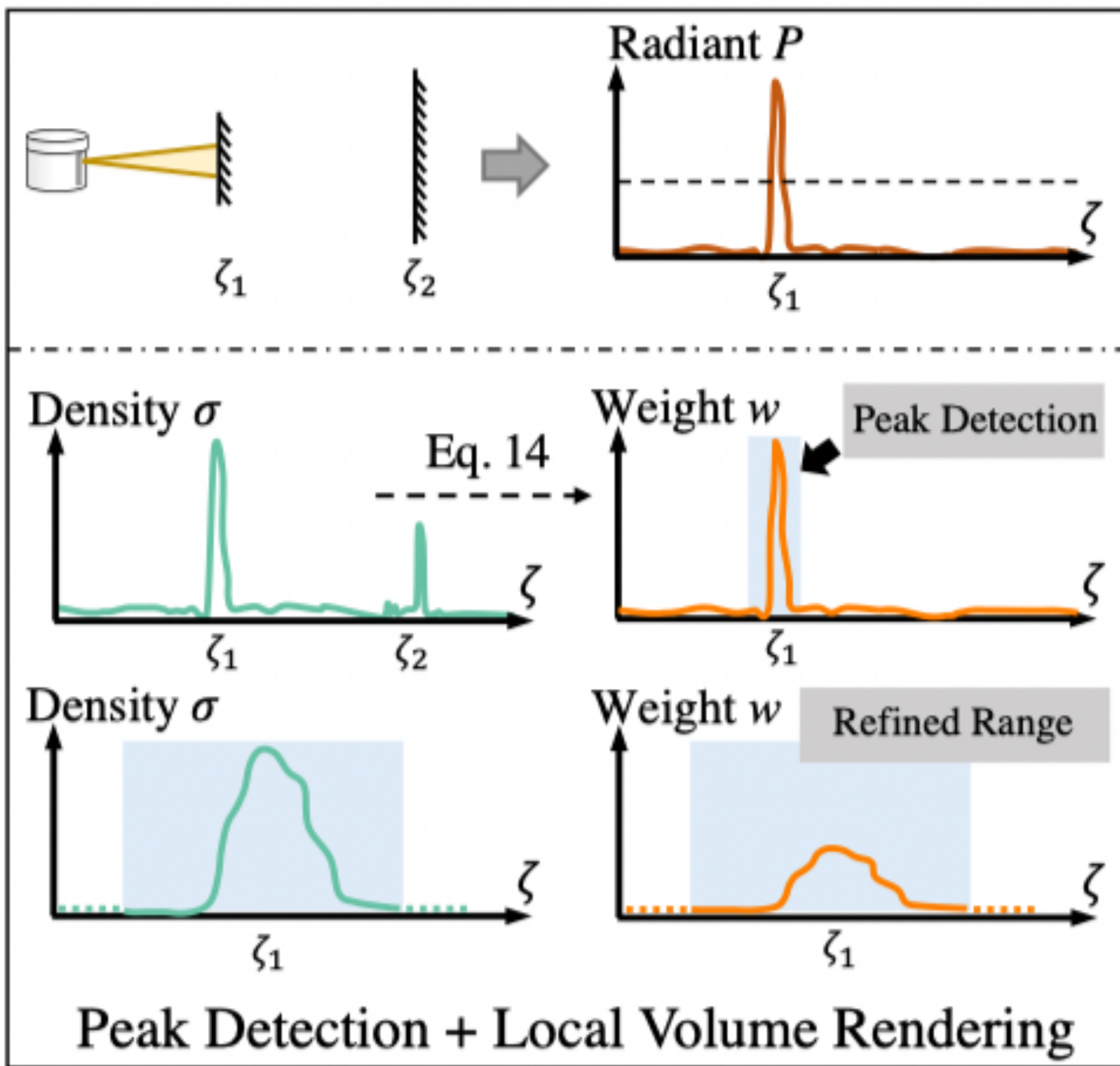
Shengyu Huang^{1,2}, Zan Gojcic², Zian Wang^{2,3,4}, Francis Williams², Yoni Kasten², Sanja Fidler^{2,3,4}, Konrad Schindler¹, Or Litany²ETH Zürich¹NVIDIA²University of Toronto³Vector Institute⁴**Problem statement**

- Input:** LiDAR scans $\mathbf{X} = \{\mathbf{X}_v\}_{v=1}^{n_v}$, where each scan \mathbf{X}_v is associated with a sensor pose $\mathbf{T}_v \in \text{SE}(3)$ and consists of n_r rays. Every ray $\mathbf{r}(\mathbf{o}, \mathbf{d})$ records observations $(\zeta_1, e_1, p_d, p_s, \zeta_2, e_2)$ as:
 - ζ_* : range of the first/second return
 - e_* : intensity of the first /second return
 - $p_d \in [0,1]$: ray drop probability
 - $p_s \in \{0,1\}$: two return mask

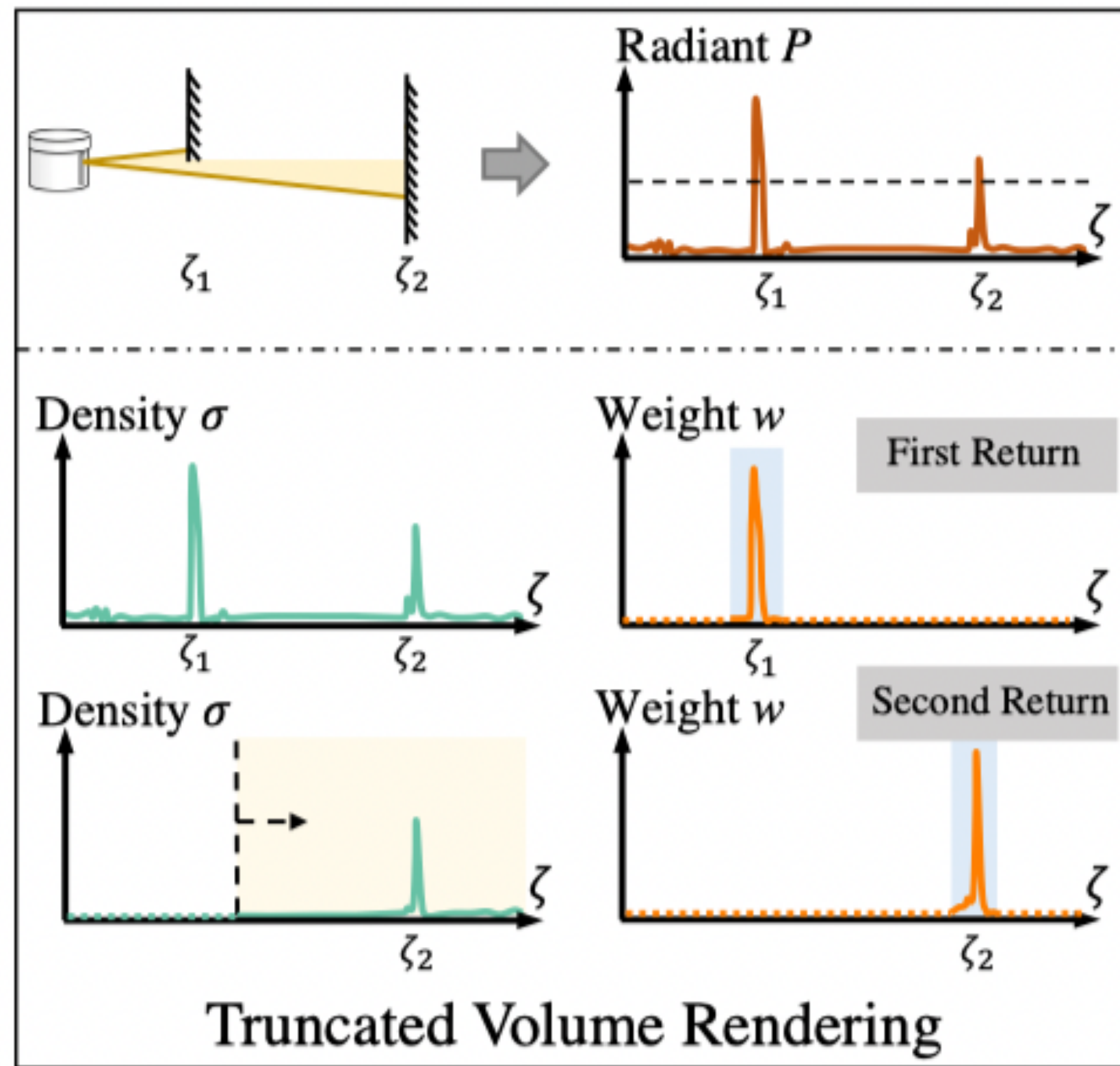
- Goal:** reconstruct the scene, render virtual LiDAR scans \mathbf{X}_{tgt} from novel sensor poses \mathbf{T}_{tgt}

Methodology

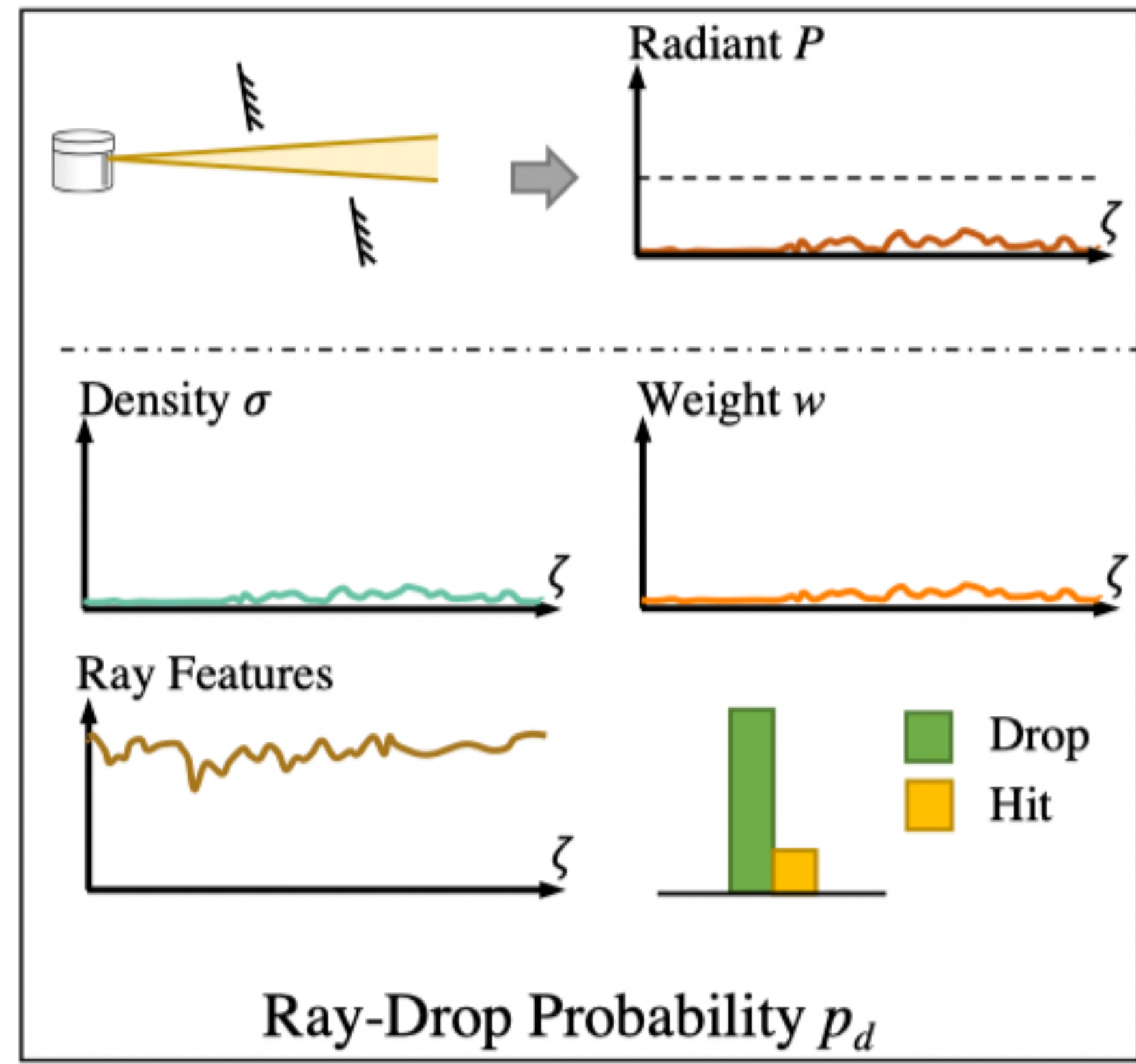
First return range estimation



Second return range estimation



Ray drop estimation

**Volume rendering for LiDAR rays**

- Range dependent received radiant power $P(\zeta)$:

$$P(\zeta) = \int_0^{2\zeta/c} P_e(t) H(\zeta - \frac{ct}{2}) dt, \quad H(\zeta) = H_T(\zeta) H_C(\zeta)$$

- Target response $H_T(\zeta)$ and receiver response $H_C(\zeta)$:

$$H_T(\zeta) = \frac{\rho}{\pi} \cos(\theta) \delta(\zeta - \zeta_0), \quad H_C(\zeta) = T_\zeta^2 \frac{A_e}{\zeta^2}$$

- Probabilistic radiant power P_ζ at range ζ :

$$P_\zeta = C \frac{T_\zeta^2 \cdot \sigma_\zeta \rho_\zeta}{\zeta^2} \cos(\theta),$$

- Volume rendered observed power P :

$$P = \sum_{j=1}^N \int_{\zeta_j}^{\zeta_{j+1}} C \frac{T_\zeta^2 \cdot \sigma_\zeta \rho_\zeta}{\zeta^2} \cos(\theta_j) d\zeta = \sum_{j=1}^N w_j p'_j$$

Core difference

$$w_j = 2\alpha_{\zeta_j} \cdot \prod_{k=1}^{j-1} (1 - 2\alpha_{\zeta_k}), \quad \text{Ours}$$

$$w_j = \alpha_{\zeta_j} \cdot \prod_{k=1}^{j-1} (1 - \alpha_{\zeta_k}), \quad \text{NeRF}$$

Experimental results

Results of LiDAR range, intensity and ray drop estimation

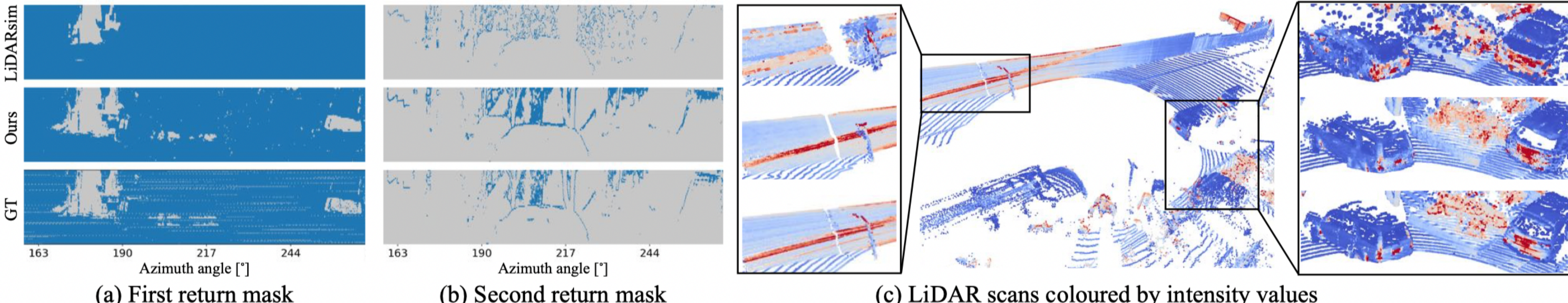
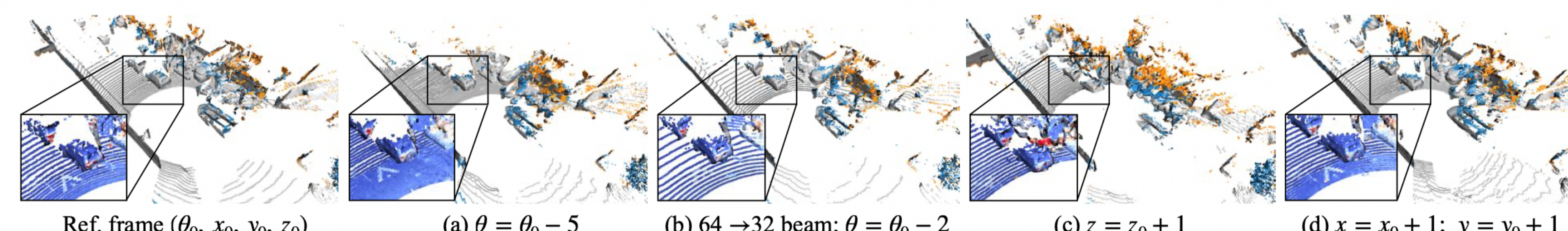


Figure 3. Qualitative results of LiDAR novel view synthesis on Waymo Interp. dataset. On the left, we color-code rays with and without return. On the right side, LiDAR intensity values are color-coded as :0 0.25.

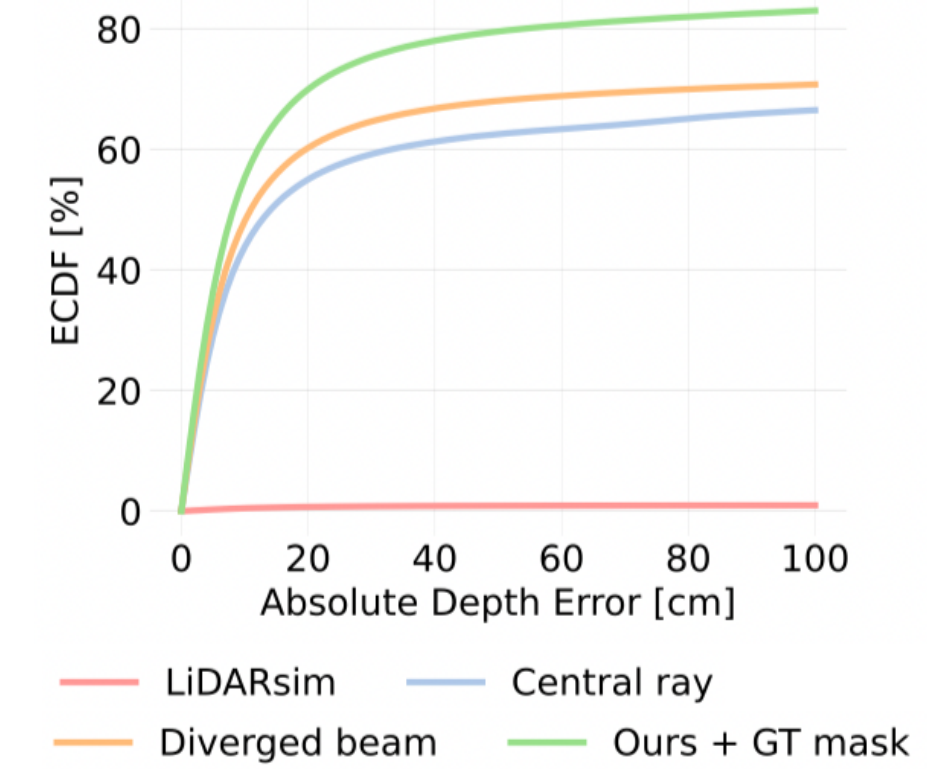
Method	First range			Second range			Intensity			Ray drop			
	Recall@50↑	MAE↓	MedAE↓	Seg. recall↑	Seg. precision↑	Recall@50↑	MAE↓	MedAE↓	MAE ^{1st} ↓	MAE ^{2nd} ↓	Recall↑	Precision↑	IoU↑
LiDARsim [24]	74.1	105.4	18.5	3.5	11.5	1.0	2258.0	1898.2	0.013	0.018	32.5	85.5	30.5
Central ray	92.8	32.8	5.6	79.8	62.9	61.1	589.1	21.8	0.004	0.009	64.3	81.7	57.1
Ours	92.3	36.1	5.7	82.1	55.6	67.4	505.1	13.4	0.004	0.008	65.1	78.0	56.1
Diverged beam	93.2	29.7	5.6	100.0	100.0	79.8	116.0	8.1	0.004	0.011	65.1	78.0	56.1
GT mask	93.2	29.7	5.6	100.0	100.0	79.8	116.0	8.1	0.004	0.011	65.1	78.0	56.1

Table 1. Comprehensive ray measurement evaluation of LiDAR novel view synthesis on Waymo Interp. dataset.

- LiDAR novel view synthesis (more in our project page!)

Figure 5. LiDAR novel view synthesis by changing the sensor elevation angle θ [$^\circ$], pose (x, y, z) [m] and number of beams. Zoom-in points are color-coded by intensity values.

Improved second range



Effectiveness of volume rendering for LiDAR rays

Method	TownClean			Waymo Interp.		
	MAE ↓	MedAE ↓	CD ↓	MAE ↓	MedAE ↓	CD ↓
i-NGP [30]	41.0 (-1.2)	4.1 (0.0)	17.6 (0.2)	25.3 (-1.1)	4.5 (-1.0)	10.5 (-1.1)
DS-NeRF [8]	37.4 (-4.2)	3.0 (-0.9)	14.4 (-2.2)	27.4 (-0.8)	5.4 (-1.0)	13.6 (-0.9)
URF [38]	46.4 (3.0)	4.5 (0.3)	18.4 (1.6)	28.3 (0.1)	5.3 (-0.1)	13.1 (0.2)
Ours	32.0 (-2.1)	2.3 (-2.5)	9.0 (-3.9)	30.8 (-2.1)	5.1 (-2.0)	12.1 (-2.3)

Table 3. Ablation study of volume rendering for active sensing.

Downstream evaluation of novel views

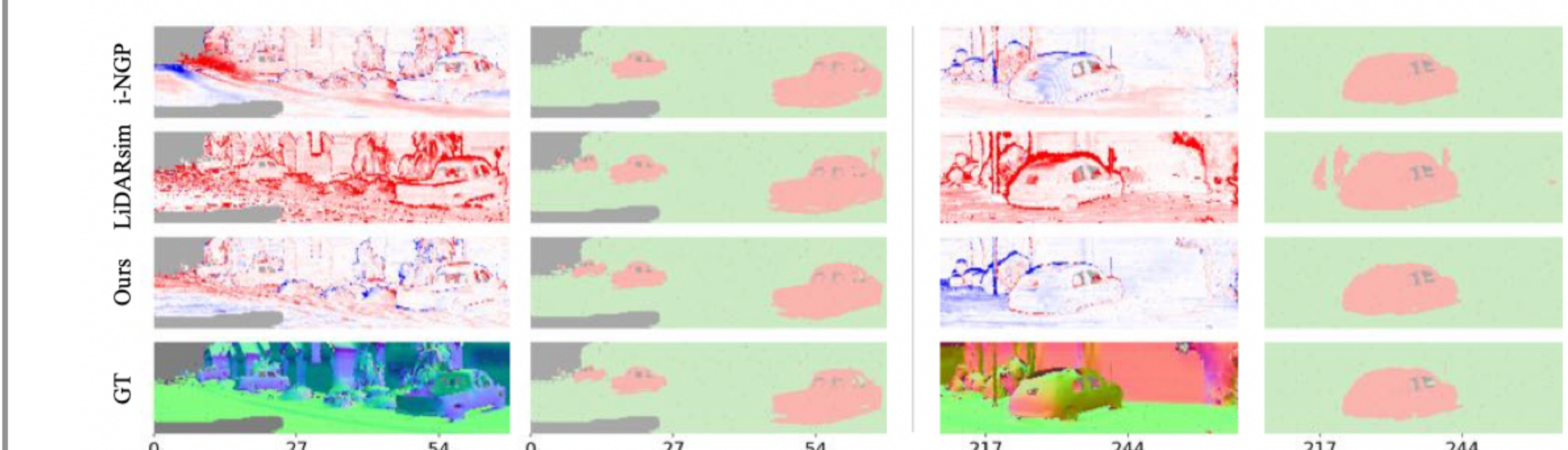


Figure 7. Semantic segmentation results on synthesised Waymo NVS dataset. Geometry inaccuracy (-100 - 100 cm) leads to erroneous semantic segmentation (dropped rays, vehicle, pedestrian, background).